Angewandte Chemie
Eine Zeitschrift der Gesellschaft Deutscher Chemiker

Supporting Information

Bifunctional Metal–Organic Framework Synergistically Enhances Radiotherapy and Activates STING for Potent Cancer Radio-Immunotherapy

C. Wang, J. Li, X. Jiang, X. Ma, W. Zhen, L. Tillman, R. R. Weichselbaum, W. Lin**

Supporting Information for

Bifunctional Metal-Organic Framework Synergistically Enhances Radiotherapy and Activates STING for Potent Cancer Radio-Immunotherapy

Chaoyu Wang[a][b][+], Jinhong Li[a][+], Xiaomin Jiang[a][b][+], Xin Ma[a], Wenyao Zhen[a][b], Langston Tillman[a], Ralph R. Weichselbaum [b]*, Wenbin Lin [a][b]*

[a]Department of Chemistry, The University of Chicago, Chicago, IL 60637, USA
[b]Department of Radiation and Cellular Oncology and Ludwig Center for Metastasis Research, The University of Chicago, Chicago, IL 60637, USA

[+]These authors contributed equally.

*Corresponding author
Email: wenbinlin@uchicago.edu; rweichselbaum@uchicagomedicine.org

1. Experiment Section

1.1. Ethical statement

This research complies with all relevant ethical regulations. All work performed on animals was in accordance with and approved by the Institutional Animal Care and Use Committee at the University of Chicago. The approved number is 72408. Animals were housed in 12 light/12 dark cycle, 65-75°F (~18-23°C), and 40-60% humidity condition. Animals were euthanized when the tumor reached 20 mm in any dimension or when they became moribund with severe weight loss or unhealing ulceration. This limit was not exceeded at any point.

1.2. Synthesis and characterization of MOF/MSA-2

Starting materials for HCBB ligand and Hf-HCBB MOF synthesis and other reagents were purchased from Sigma-Aldrich and ThermoFisher (USA) unless otherwise noted and used without further purification. Transmission electron microscopy (TEM) was performed on a TECNAI Spirit microscope. Powder X-ray diffraction (PXRD) patterns were acquired on a Bruker D8 Venture diffractometer using a Cu Kα radiation source (λ = 1.54178 Å) and processed with PowderX software. UV-Vis spectra were obtained with a Shimadzu UV-2600 UV-Vis spectrophotometer. Dynamic light scattering (DLS) and ζ-potential were measured on a Malvern Zetasizer Nano ZS instrument. ^{1}H-NMR spectra were collected on a Bruker NMR 400 DRX spectrometer at 400 MHz. The concentration of MSA-2 was quantified by LC-MS on an Agilent 6540 Q-tof system with Agilent ZORBAX Extend-C18 Column (2.1 mm × 50 mm, 3.5 μm). N_2 sorption isotherms for 77 K were measured with a Micromeritics 3Flex adsorption analyzer.
Synthesis of HCBB ligand. HCBB ligand was synthesized according to the literature reports[1]. ^{1}H NMR (400 MHz, DMSO): δ 12.87 (br, s), δ 7.85 (d, J = 8.1 Hz, 12H), 7.58 (d, J = 8.2 Hz, 12H), 7.36 (d, J = 8.1 Hz, 12H), 7.14 (d, J = 8.0 Hz, 12H).

Synthesis of Hf-HCBB MOF and MOF/MSA-2. 500 μL of $HfCl_4$ solution (8.28 mg/mL in DMF), 500 μL of HCBB solution (4.66 mg/mL in DMF), 35 μL of acetic acid, and 7.5 μL of water were added to a 1-dram glass vial. The mixture was sonicated and heated in an 80 °C oven for 24 h. The white suspension was collected by centrifugation and washed with DMF, 10% triethylamine solution in ethanol, and ethanol. The final product was dispersed in ethanol for storage. Yield: 3.2 mg (67.5%). This reaction was also performed by adding 629 mg $HfCl_4$, 354 mg HCBB ligand, 152 mL DMF, 5.32 mL HOAc, and 1140 uL H_2O. After stirring in 80 ℃ for 48 h, 533 mg MOF was obtained in a yield of 72% (Figure S14).

To prepare MOF/MSA-2, the MOF was dispersed in ethanol at an equivalent Hf concentration of 1.9 mM, and an equivalent volume of MSA-2 solution (0.63 mg/mL in ethanol) was added to the MOF suspension. The mixture was heated at 50 °C and vortexed overnight to afford MOF/MSA-2. White precipitates of MOF/MSA-2 were collected by centrifugation, washed twice with water, and dispersed in water for storage. Yield: 89%.

LC-MS quantification of MSA-2. LC-MS quantification of MSA-2 was performed on an Agilent 6540 Q-Tof system. with a mobile phase A (0.1% TFA in water [v/v]) and mobile phase B (0.1% TFA in acetonitrile [v/v]). The column temperature and sample temperature were both room temperature. The injection volume was 20 μL. For release studies, MOF/MSA-2 was incubated with 0.1× and 1× PBS for different lengths of time. The mixture was centrifuged at 14,000 rpm for 15 minutes, and the supernatant was diluted with water first and then subjected to LC-MS to quantify the concentrations of released MSA-2.

Digestion of MOF and MOF/MSA-2 for NMR studies. 200 μL of MOF or MOF/MSA-2 suspension was centrifuged and dried under vacuum and then digested in a mixture of 450 μL DMSO-*d*$_6$ and 50 μL concentrated D_2SO_4 by sonication for 10 minutes. The samples were used directly for ^{1}H NMR characterization.

1.3. X-ray irradiation and biological studies

For X-ray irradiation in test tubes and in vitro experiments, an RT250 orthovoltage X-ray machine model (Philips, USA) with a fixed setting at 250 kVp, 15 mA, and a built-in 1 mm Cu filter was used. Throughout the studies, all cells were tested negative for mycoplasma contamination and morphologically confirmed.

1.4. ROS generation

To image ROS generation in cells, 50,000 CT26 cells were incubated with indicated samples containing 10 μM MSA-2 at 37 °C for 24 h. The medium was replaced with fresh medium containing DCFH-DA (1:2000 dilution). Selected groups were irradiated with 2 Gy of X-rays. After incubation for 20 min at 37 °C, the cells were washed with PBS, stained with DAPI, and then imaged with a Leica SP8 confocal microscope.

1.5. Measurement of ICD markers

50,000 CT26 cells were treated with indicated samples containing 10 μM MSA-2 for

24 h. Selected groups were irradiated with 2 Gy of X-rays. The cells were cultured at 37 °C for 24 h.
To characterize the CRT on the surface of CT26 cells, the cells were incubated with an anti-calreticulin-488 (Cell Signaling Technology, 1:200) to label the CRT following the manufacturer's instructions. The cells were washed with PBS, stained with Hoechst 33342 to label the nuclei, and then imaged on a confocal microscope (Leica SP8).
To determine HMGB1 release, the medium was collected and centrifuged (14000 g, 10 min) to obtain the supernatant. HMGB1 in the supernatant was detected by ELISA kit (Chondrex, USA) according to the manufacturer's instructions.
To determine ATP secretion, the medium was collected and centrifuged (14000 g, 10 min) to obtain the supernatant. The ATP in the supernatant was determined by the ATP detection kit according to the manufacturer's instructions.

1.6. Confocal imaging of γ-H2AX

50,000 CT26 cells were treated with indicated samples containing 10 μM MSA-2 for 24 h. Selected groups were irradiated with 2 Gy of X-rays. The cells were cultured at 37 °C for 24 h and then incubated with Phalloidin (F-actin, Cell Signaling Technology, 1:20) to label the cytoskeleton and an anti-γ-H2AX (Cell Signaling Technology, 1:200) and secondary antibody Alexa Fluor 594 antibody (Cell Signaling Technology, 1:200) to label the γ-H2AX following the manufacturer's instructions. The cells were washed with PBS, stained with Hoechst 33342 to label the nuclei, and then imaged on a Leica Stellaris 8 confocal microscope.

1.7. STING activation in vitro

THP1-Dual™ KO-MyD88 reporter cells were used to quantify STING activation in vitro. The cells were seeded in 96-well plates at a density of 2×10^5 cells/mL (n = 3), and 0.39-150 μM MSA-2 or MOF/ MSA-2 was added and incubated for 24 hours. The stimulation of the IRF pathway was quantified by QUANTI-Luc (InvivoGen) assay on a Synergy HTX plate reader. The cytokines secreted in the medium were quantified by LumiKine™ Xpress mIFN-β 2.0 (InvivoGen), SUP mouse ELISA kit (Invitrogen), or IL-6 mouse ELISA kit (Invitrogen).

1.8. Western blotting

In vitro cell samples harvested on indicated days were lysed using the radioimmunoprecipitation assay (RIPA) buffer in the presence of protease and phosphatase inhibitor cocktail. The protein concentration was quantified using a Pierce BCA protein kit (Thermo Fisher Scientific). Equal amounts of samples (30 μg) were separated using the SDS-polyacrylamide gel and electro-transferred to polyvinylidene fluoride membranes. Membranes were blocked with 5% non-fat milk in tris-buffered saline containing 0.1% Tween 20 before incubation at 4 °C overnight with the following primary antibodies: β-actin (1:1000), γ-H2AX (1:1000), STING (1:1000), phospho-STING (1:1000), IRF3 (1:1000), and phospho-IRF3 (1:1000). The membranes were further incubated with corresponding horseradish peroxidase-conjugated secondary

antibodies (1:10000) at room temperature for 1 h. After extensive washing with TBST, the membranes were incubated with Pierce ECL Plus Western blotting substrate (Thermo Fisher Scientific, USA) and visualized using a FluorChem R system (ProteinSimple, USA).

1.9. In Vivo antitumor efficacy

For studies with CT26 tumors, Balb/c mice were subcutaneously inoculated with 2×10^6 CT26 cells on the right flanks on day 0. On day 9, tumor-bearing mice were intratumorally injected with indicated treatments containing 0.5 mg MSA-2 and/or 1.2 mmol MOF. On days 10 to 12, the tumor regions in selected groups were irradiated with 2 Gy of X-rays. Tumor size was monitored every other day, and the tumor volume was calculated by the following equation[2]: tumor volume = length×width^2×0.5. Tumor growth inhibition (TGI) was calculated using the formula: 100 - [ΔT/ΔC * 100], where ΔT is the volume change for treated tumors, and ΔC is the volume change for control tumors. On day 60, the mice with tumors completely regressed were rechallenged by subcutaneous injection of 2×10^6 CT26 tumor cells on the left flanks, and age-matched naïve mice were used as control.

For studies with bilateral MC38 tumors, C57BL/6 mice were subcutaneously inoculated with 2×10^6 MC38 cells on the right flanks and 1×10^6 MC38 cells on the left flanks on day 0. On day 8, tumor-bearing mice were intratumorally injected with indicated treatments containing 0.5 mg MSA-2 and/or 1.2 mmol MOF. On days 9 to 12, the tumor regions in the right flanks in selected groups were irradiated with 2 Gy of X-rays. On days 7 and 12, aPD-L1 (75 μg/mouse) was i.p. injected for indicated groups. Tumor growth was monitored as described above. On day 60, the mice with tumors completely regressed were rechallenged by subcutaneous injection of 2×10^6 MC38 cells in the left flanks, and age-matched naïve mice were used as control.

1.10. In Vivo antitumor immune response

BALB/c mice bearing subcutaneous CT26 tumors were randomly grouped and intratumorally injected with indicated treatments containing 0.5 mg MSA-2. On days 10 to 12, the tumor regions in selected groups were irradiated with 2 Gy of X-rays. Two days after the last X-ray treatment, the mice were sacrificed to harvest the tumors and TDLNs for innate immune cell profiling.

C57BL/6 mice bearing subcutaneous MC38 tumors were randomly grouped and intratumorally injected with indicated treatments containing 0.5 mg MSA-2. On days 9 to 12, the tumor regions in selected groups were irradiated with 2 Gy of X-rays. Five days after the last X-ray treatment, the mice were sacrificed to harvest the primary and distant tumors for adaptive immune cell profiling

For flow cytometry analysis, tumor tissues and tumor-draining lymph nodes were harvested from tumor-bearing mice and cut into small pieces, followed by digestion using the digestion buffer (1 mg/ml collagenase and 100 μg/ml deoxyribonuclease I in serum-free RPMI) at 37℃ with gentle shaking for 30 min. The suspension was passed through a 70-μm strainer to obtain the single-cell suspension. The cells were incubated with CD16/32 (1:20) for 10 min and then incubated with anti-CD45-BV 421 (1:100),

anti-CD3e-PE-Cy7 (1:100), anti-NK1.1-PE Dazzle 594 (1:100), anti-B220-APC (1:100), anti-CD4-APC-Cy7 (1:100), anti-CD8α-PerCP-eFluor 710 (1:100), anti-CD62L-FITC (1:100), anti-CD44-PE (1:100), anti-CD11b-FITC (1:100), anti-F4/80-PerCP-Cy5.5 (1:100), anti-Gr-1-PE (1:100), anti-CD206-PE-Cy7 (1:100), anti-CD86-APC (1:100), anti-CD3e-PE-eFluor 610 (1:100), anti-CD11c-PE-Cy5.5 (1:100), anti-MHCII-PE (1:100) before flow cytometry. The cells were analyzed by flow cytometry (Aurora), and the flow cytometry data were processed by FlowJo software.

1.11. Histological Assay

The excised tumors and other organs were fixed with 4% neutral paraformaldehyde buffer, embedded in paraffin, and sliced into sections of 5 μm thick. The sections were subjected to H&E, Ki67, γ-H2AX, CD3e, or IBA-1 staining before histopathological examination with a Panoramic MIDI II digital slide scanner.

1.12. Statistical Analysis

Results are presented as means ± SD. Data were analyzed by one-way or two-way ANOVA, followed by Tukey's multiple comparisons post-test with Prism 8.0 (GraphPad Software). P values less than 0.05 were considered statistically significant. All values are reported as means ± SD unless specified otherwise.

2. Supporting Figures and Tables

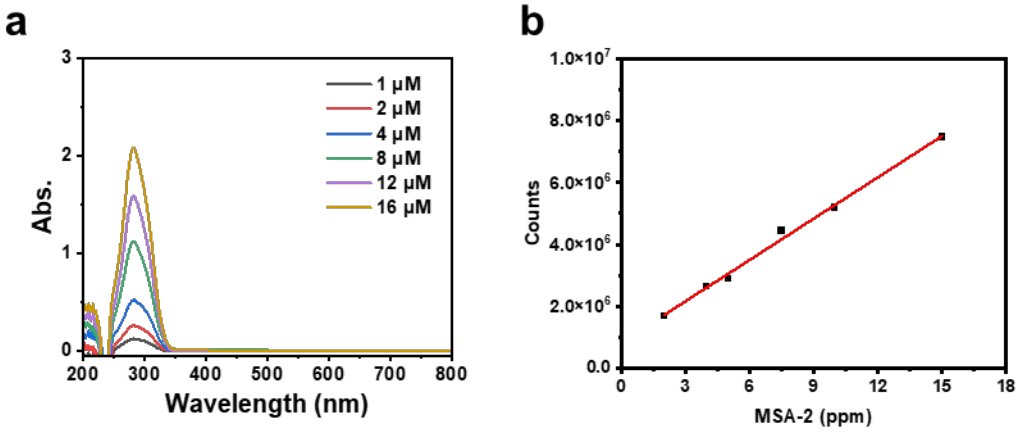

Figure S1. (a) UV standard curve of HCBB ligand. (b) LC-MS standard curves of MSA-2.

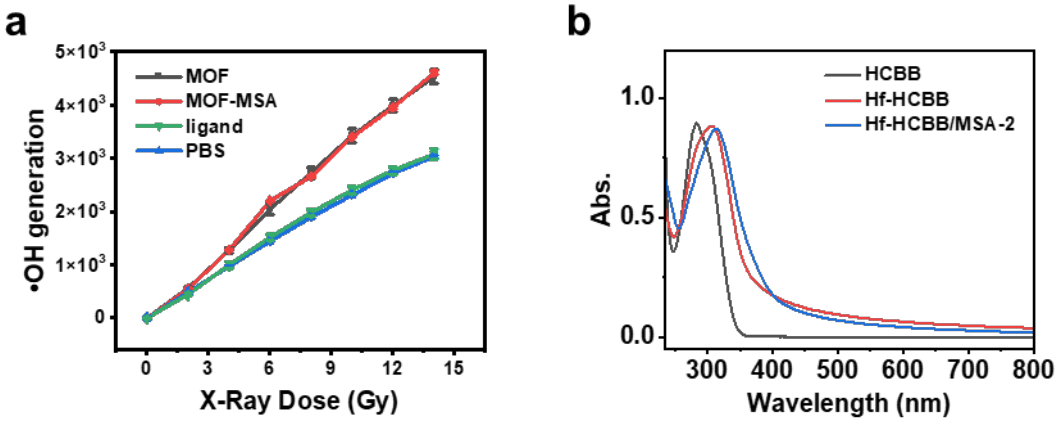

Figure S2. (a) Hydroxyl radical signals of PBS, HCBB ligand, Hf-MOF, and Hf-MOF-MSA by APF assays after different doses of X-ray radiation, n=3. (b) UV−visible absorption spectra of HCBB ligand, Hf-MOF, and Hf-MOF/MSA-2 in EtOH.

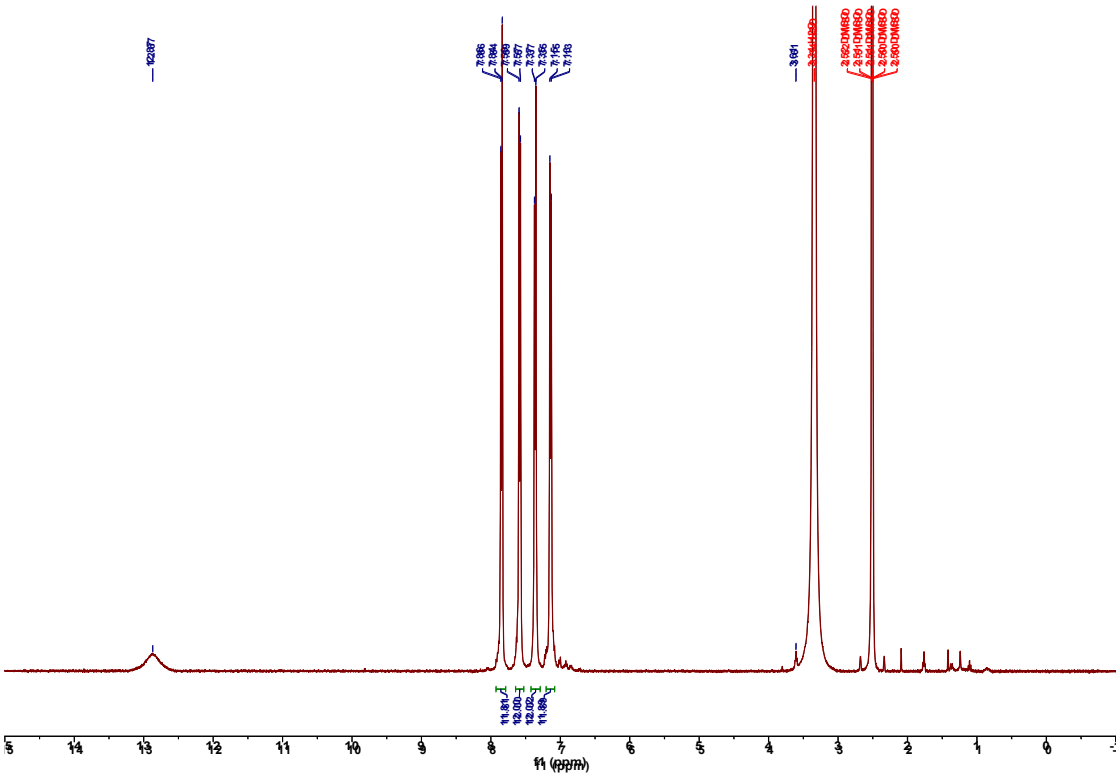

Figure S3. ^{1}H NMR spectrum of HCBB in DMSO-d_6 (400 MHz).

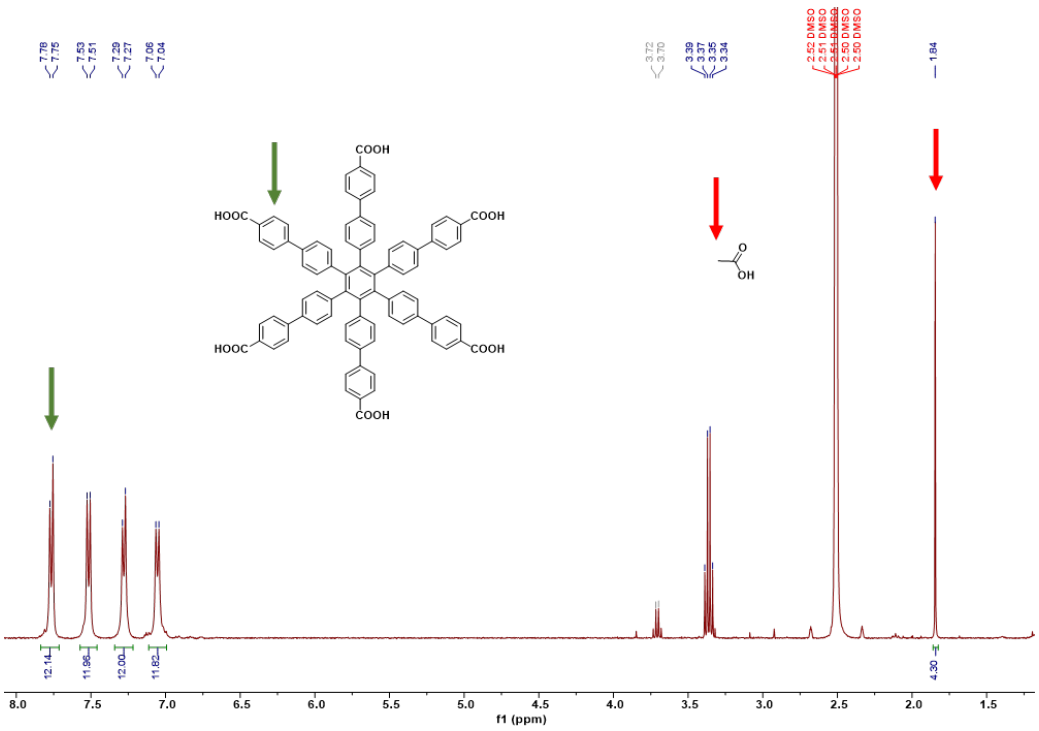

Figure S4. ^{1}H NMR spectrum of digested Hf-HCBB MOF in D_2SO_4/DMSO-d_6 (400 MHz).

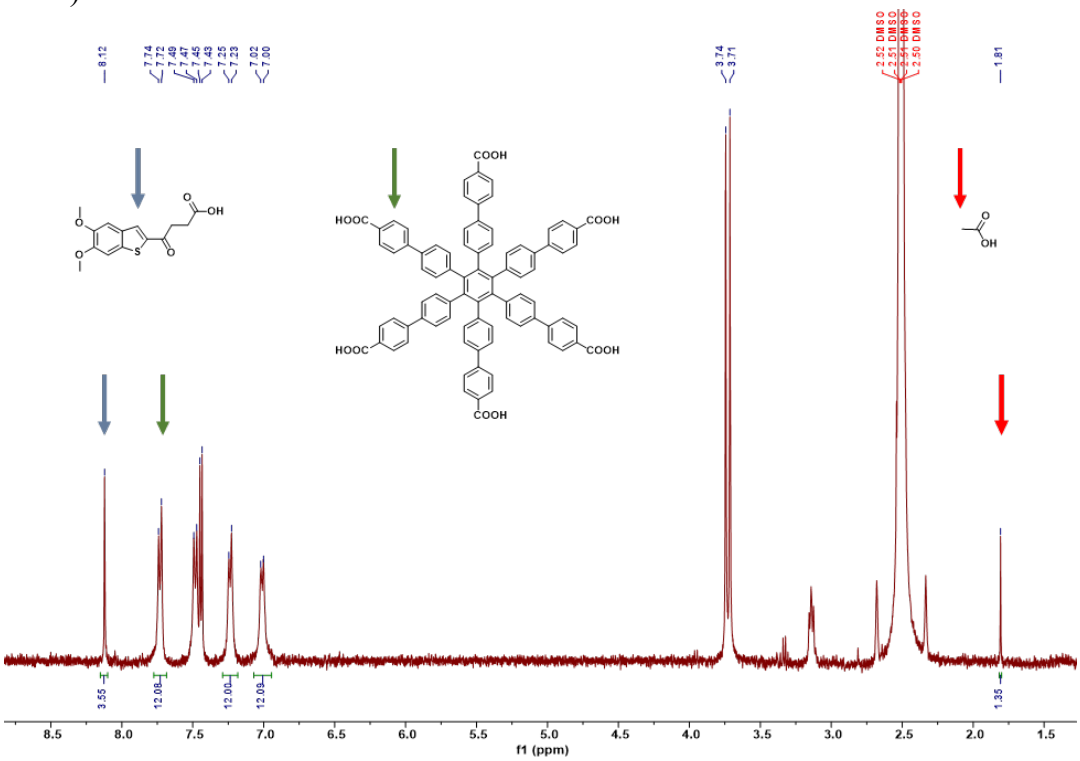

Figure S5. ^{1}H NMR spectrum of digested MOF/MSA-2 in D_2SO_4/DMSO-d_6 (400 MHz).

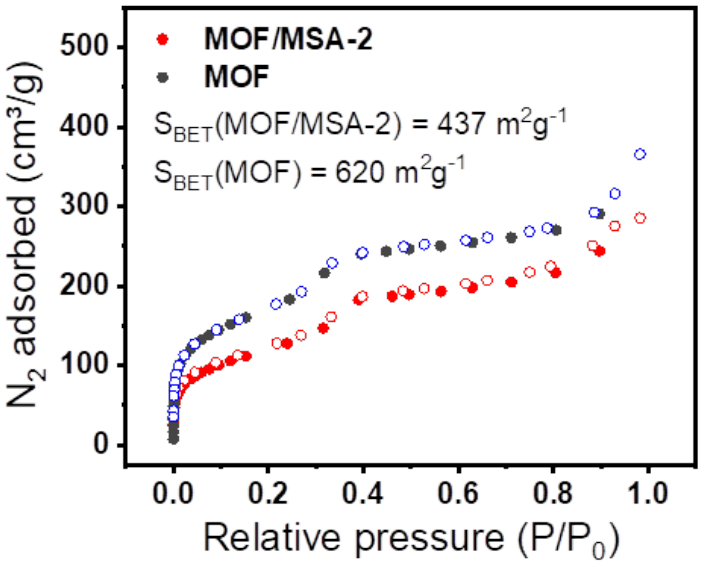

Figure S6. Nitrogen sorption isotherms for MOF and MOF/MSA-2 at 77 K. The Brunauer-Emmett-Teller (BET) surface area of the MOF is lower than the reported values due to the small particle size in our sample[3]. The decrease in the BET surface area of MOF/MSA-2 is consistent with the loading of MSA-2.

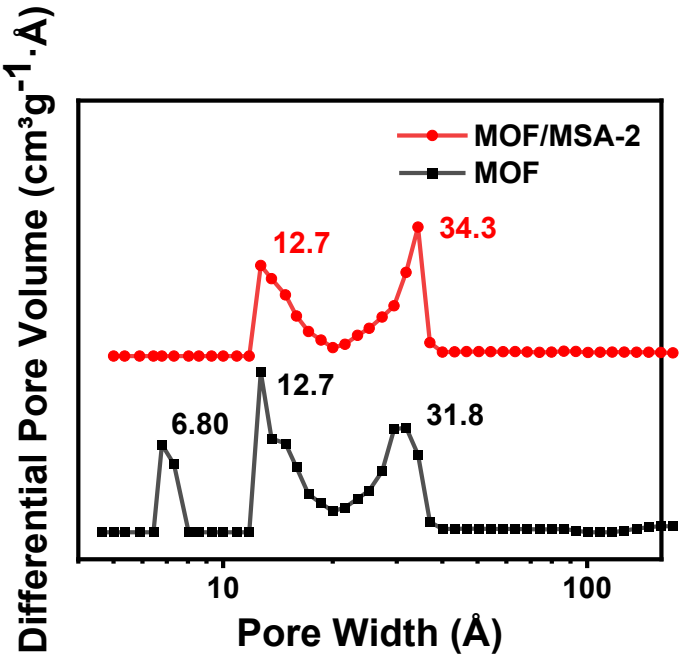

Figure S7. Pore size distributions of MOF and MOF/MSA-2 calculated by the DFT method. The pores around 12.7 Å match the expected pores based on the structural models of the MOFs and previous literatures[3]. The larges pores of 31.8 Å and 34.3 Å for MOF and MOF/MSA-2, respectively, can be attributed to the interparticle gaps in the bulk samples due to the small particle sizes of MOF and MOF/MSA-2.

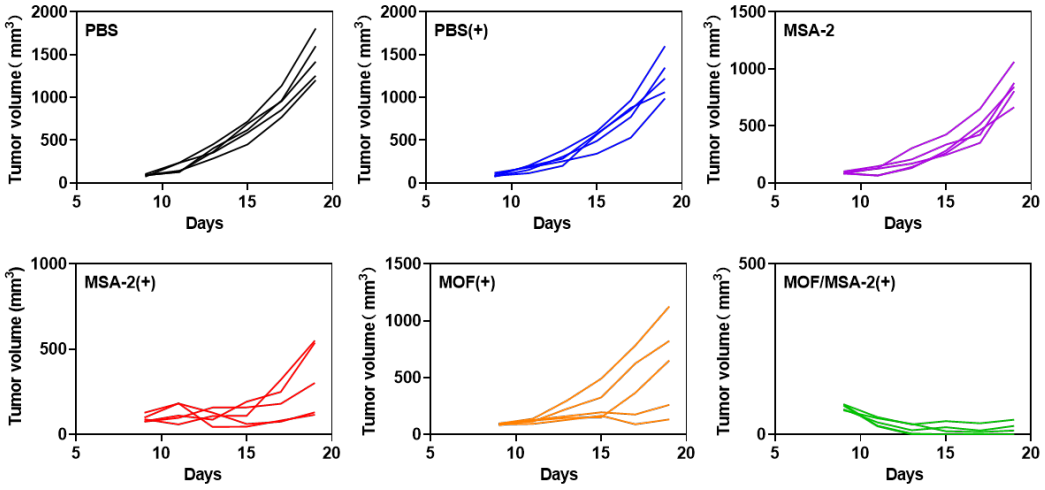

Figure S8. Individual tumor growth curves for CT26 tumor-bearing mice after different treatments (n = 5 mice per group).

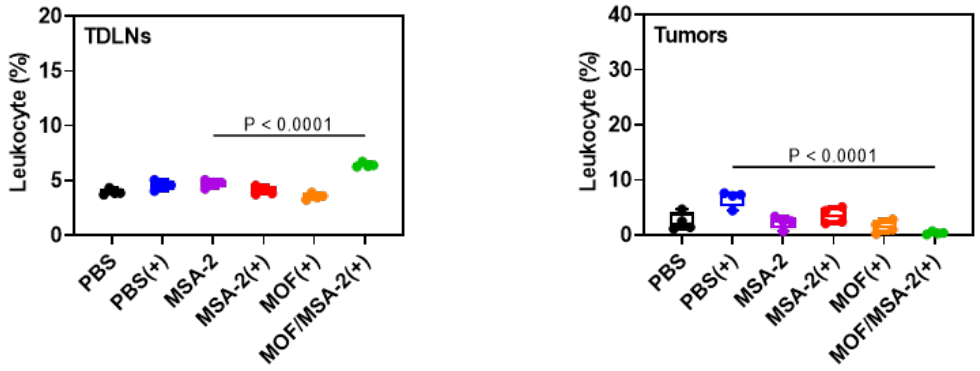

Figure S9. Leukocytes are marked by $CD45^{+}$.

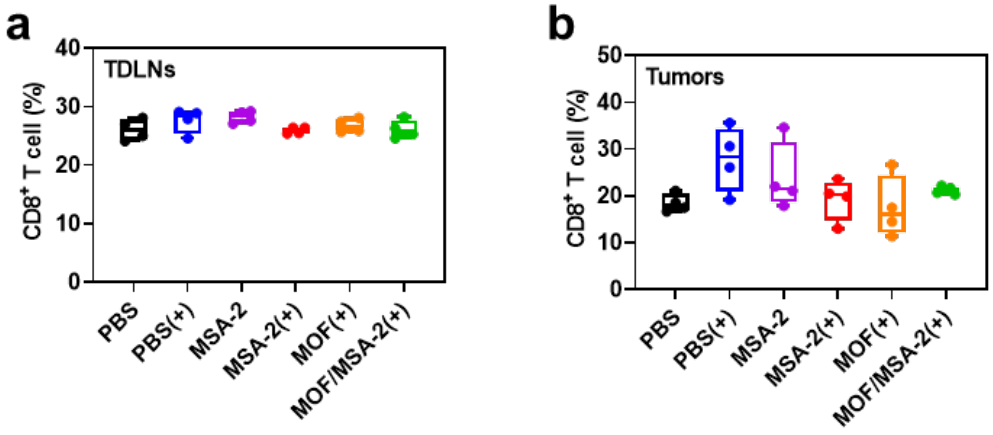

Figure S10. Immune cell infiltration into TDLNs and tumors on day 14 (2 days after the last dose of X-ray) quantified by flow cytometry. (a,b) In TDLNs and tumors, $CD8^{+}$ T cell subpopulations are defined as: $CD45^{+}$ $CD3e^{+}$ $CD8^{+}$. (ANOVA with Tukey test, n = 4).

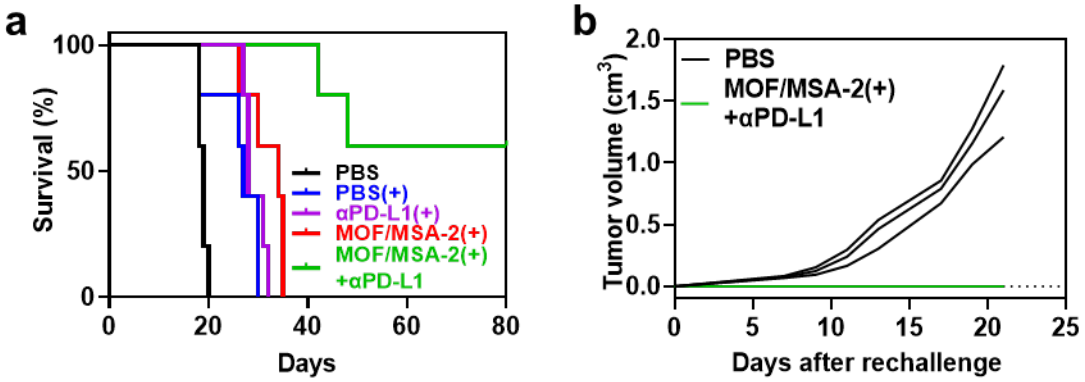

Figure S11. Mouse survival and tumor rechallenge study. (a) Mouse survival after different treatments. (b) Tumor-free mice in the MOF/MSA-2(+)+αPD-L1 group were rechallenged with MC38 cells on day 60 and age-matched untreated mice were used as control. Shown are the individual tumor growth curves post rechallenge. n = 3.

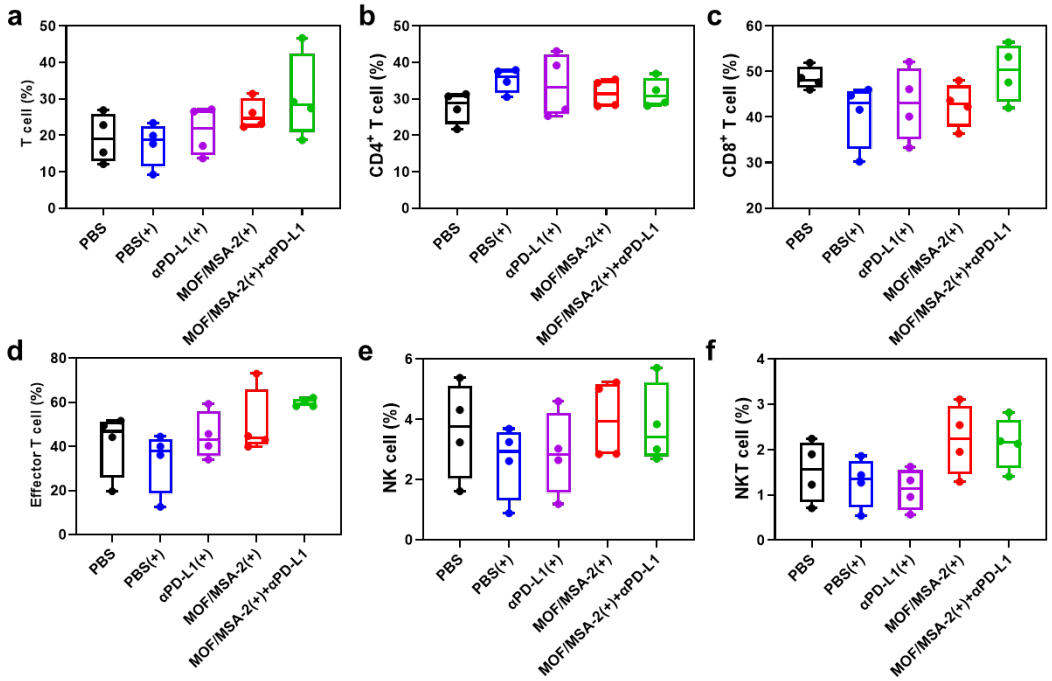

Figure S12. Immune cell infiltration into primary tumors on day 17 (5 days after the last dose of X-ray) quantified by flow cytometry. T cell subpopulations are defined as: (a) Total T cells as CD45+ CD3e+; (b) CD4+ cells as CD45+ CD3e+ CD4+; (c) CD8+ T cells as CD45+ CD3e+ CD8+; (d) Effector T cells as CD45+ CD3e+ CD44+ CD62L−; (e) NK cells as CD45+ CD3e− NK1.1+; (f) NKT cells as CD45+ CD3e+ NK1.1+ (ANOVA with Tukey test, n = 4).

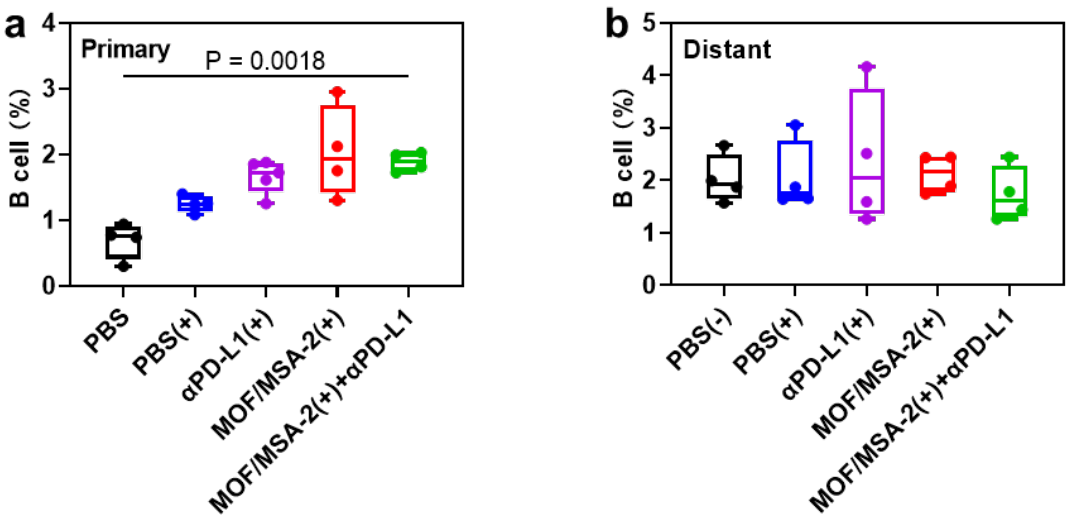

Figure S13. B cell infiltration into TDLNs (a) and tumors (b) on day 17 (5 days after the last dose of X-ray) quantified by flow cytometry. B cells are defined as $CD45^{+}$ $CD3e^{-}$ $B220^{+}$ (ANOVA with Tukey test, n = 4).

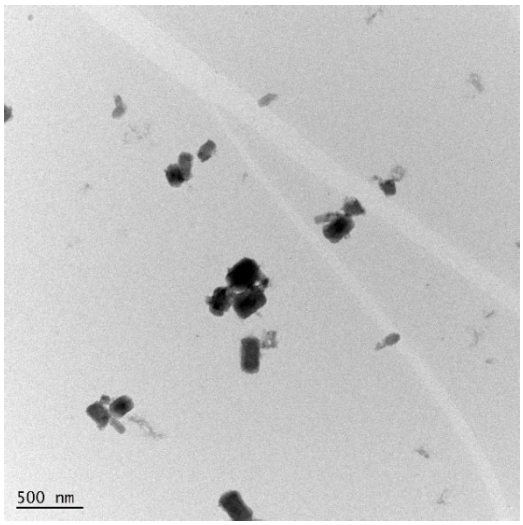

Figure S14. TEM image of Pbz-MOF from a large-scale synthesis.

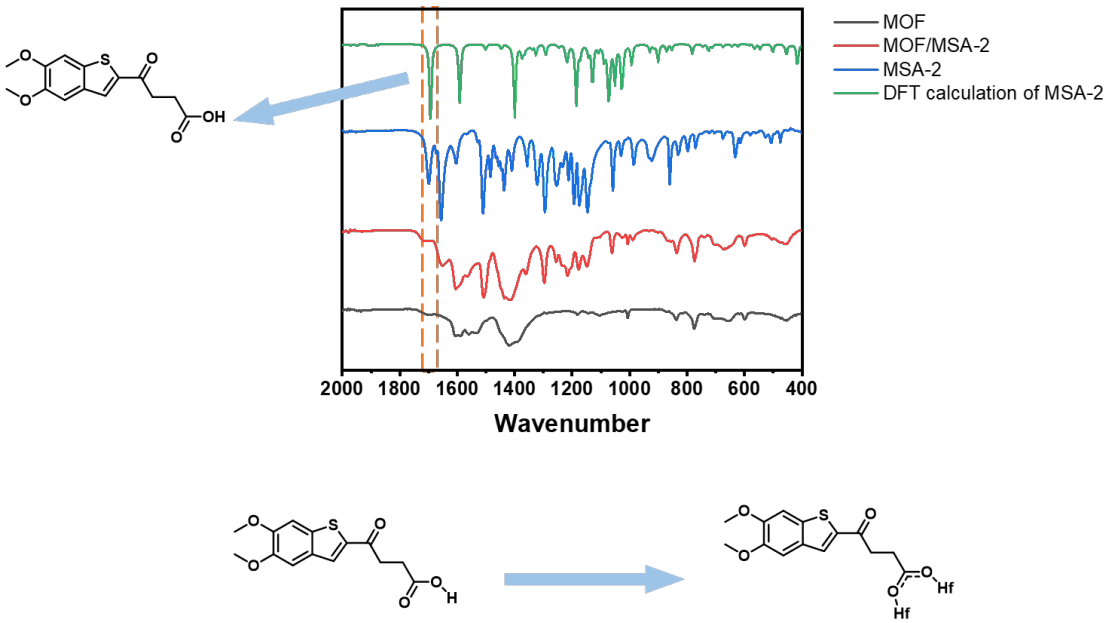

Figure S15. Fourier-transform infrared (FT-IR) spectroscopy analysis of MSA-2 coordination to Hf_6-SBUs.

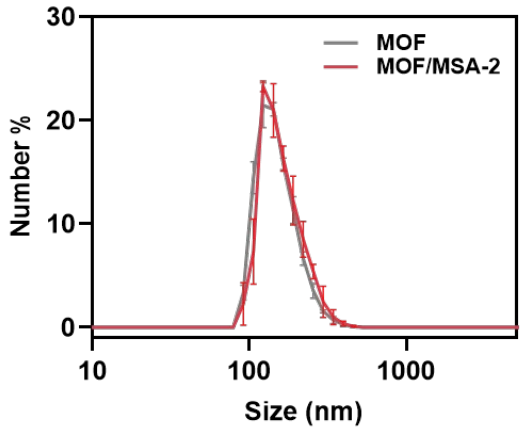

Figure S16. Number-averaged sizes of MOF and MOF/MSA-2 in cell culture medium DMEM + 10%FBS + 1%P/S. To investigate the colloidal stability, MOF or MOF/MSA-2 was incubated at 37°C for 24 hours in DMEM cell culture medium supplemented with 10% fetal bovine serum and 1% penicillin/streptomycin. DLS measurements revealed a number-averaged particle size of 191 ± 3.2 nm for the MOF and 193.1 ± 5.1 nm for MOF/MSA-2.

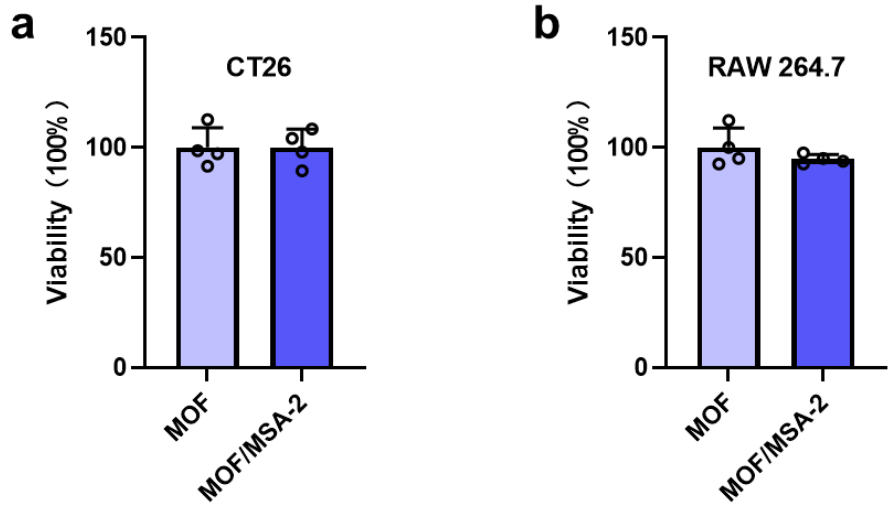

Figure S17. (a) CT26 tumor cells were treated with MOF and MOF/MSA-2 corresponding to an MSA-2 concentration of 10 μM. After 24 h, the cell viability was measured by the cell counting kit. (b) RAW 264.7 cells were treated with MOF and MOF/MSA-2 corresponding to an MSA-2 concentration of 10 μM. After 24 h, the cell viability was measured by the cell counting kit (n = 4).

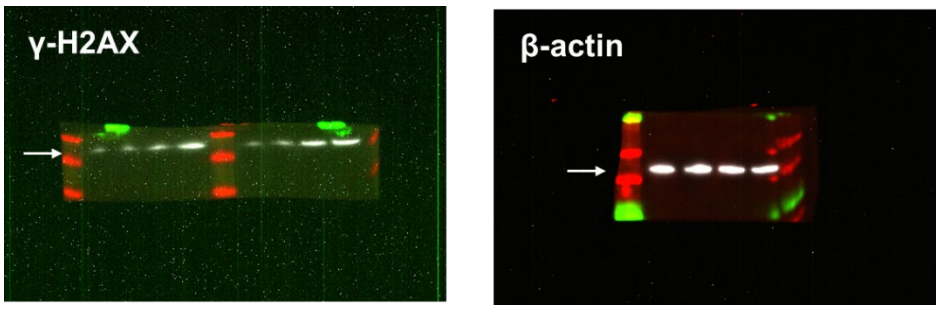

Figure S18. Uncropped/full-size blot for Figure 2c. Expression of γ-H2AX (β-actin as reference).

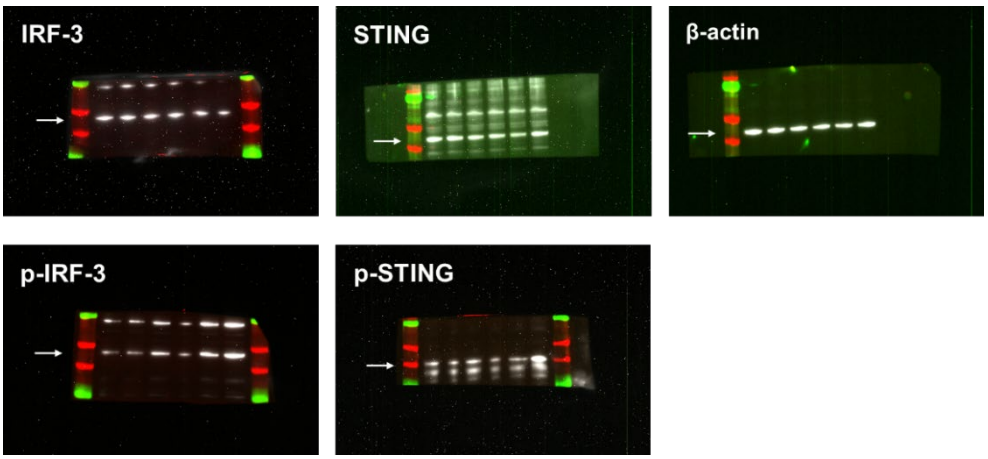

Figure S19. Uncropped/full-size blot for Figure 3b. Expression of p-IRF-3, IRF-3, p-STING, STING (β-actin as reference).

Table S1. (a-d) p-value for Figure 4 e-h.

a

Tukey's multiple comparisons test	Summary	Adjusted P Value
PBS vs. PBS(+)	ns	0.1101
PBS vs. MSA-2	*	0.0297
PBS vs. MSA-2(+)	ns	0.9829
PBS vs. MOF(+)	ns	0.5346
PBS vs. MOF/MSA-2(+)	****	<0.0001
PBS(+) vs. MSA-2	ns	0.9829
PBS(+) vs. MSA-2(+)	ns	0.3339
PBS(+) vs. MOF(+)	**	0.0033
PBS(+) vs. MOF/MSA-2(+)	****	<0.0001
MSA-2 vs. MSA-2(+)	ns	0.1101
MSA-2 vs. MOF(+)	***	0.0008
MSA-2 vs. MOF/MSA-2(+)	****	<0.0001
MSA-2(+) vs. MOF(+)	ns	0.2092
MSA-2(+) vs. MOF/MSA-2(+)	****	<0.0001
MOF(+) vs. MOF/MSA-2(+)	****	<0.0001

b

Tukey's multiple comparisons test	Summary	Adjusted P Value
PBS vs. PBS(+)	ns	0.9965
PBS vs. MSA-2	ns	0.7347
PBS vs. MSA-2(+)	ns	0.4841
PBS vs. MOF(+)	*	0.0325
PBS vs. MOF/MSA-2(+)	**	0.0053
PBS(+) vs. MSA-2	ns	0.4551
PBS(+) vs. MSA-2(+)	ns	0.7628
PBS(+) vs. MOF(+)	ns	0.0827
PBS(+) vs. MOF/MSA-2(+)	*	0.0145
MSA-2 vs. MSA-2(+)	*	0.0483
MSA-2 vs. MOF(+)	**	0.0018
MSA-2 vs. MOF/MSA-2(+)	***	0.0003
MSA-2(+) vs. MOF(+)	ns	0.6186
MSA-2(+) vs. MOF/MSA-2(+)	ns	0.1916
MOF(+) vs. MOF/MSA-2(+)	ns	0.9501

c

Tukey's multiple comparisons test	Summary	Adjusted P Value
PBS vs. PBS(+)	ns	0.9691
PBS vs. MSA-2	****	<0.0001
PBS vs. MSA-2(+)	ns	0.2269
PBS vs. MOF(+)	****	<0.0001
PBS vs. MOF/MSA-2(+)	****	<0.0001
PBS(+) vs. MSA-2	****	<0.0001
PBS(+) vs. MSA-2(+)	ns	0.6237
PBS(+) vs. MOF(+)	****	<0.0001
PBS(+) vs. MOF/MSA-2(+)	****	<0.0001
MSA-2 vs. MSA-2(+)	***	0.0001
MSA-2 vs. MOF(+)	ns	>0.9999
MSA-2 vs. MOF/MSA-2(+)	****	<0.0001
MSA-2(+) vs. MOF(+)	***	0.0002
MSA-2(+) vs. MOF/MSA-2(+)	****	<0.0001
MOF(+) vs. MOF/MSA-2(+)	****	<0.0001

d

Tukey's multiple comparisons test	Summary	Adjusted P Value
PBS vs. PBS(+)	ns	0.9983
PBS vs. MSA-2	****	<0.0001
PBS vs. MSA-2(+)	ns	0.4015
PBS vs. MOF(+)	****	<0.0001
PBS vs. MOF/MSA-2(+)	****	<0.0001
PBS(+) vs. MSA-2	****	<0.0001
PBS(+) vs. MSA-2(+)	ns	0.6373
PBS(+) vs. MOF(+)	***	0.0001
PBS(+) vs. MOF/MSA-2(+)	****	<0.0001
MSA-2 vs. MSA-2(+)	****	<0.0001
MSA-2 vs. MOF(+)	*	0.0435
MSA-2 vs. MOF/MSA-2(+)	****	<0.0001
MSA-2(+) vs. MOF(+)	**	0.0033
MSA-2(+) vs. MOF/MSA-2(+)	****	<0.0001
MOF(+) vs. MOF/MSA-2(+)	****	<0.0001

Table S2. (a-d) p-value for Figure 4 i-l.

a

Tukey's multiple comparisons test	Summary	Adjusted P Value
PBS vs. PBS(+)	ns	0.8186
PBS vs. MSA-2	*	0.0458
PBS vs. MSA-2(+)	ns	0.7535
PBS vs. MOF(+)	**	0.003
PBS vs. MOF/MSA-2(+)	**	0.0011
PBS(+) vs. MSA-2	ns	0.382
PBS(+) vs. MSA-2(+)	ns	>0.9999
PBS(+) vs. MOF(+)	*	0.0387
PBS(+) vs. MOF/MSA-2(+)	*	0.0147
MSA-2 vs. MSA-2(+)	ns	0.4498
MSA-2 vs. MOF(+)	ns	0.7758
MSA-2 vs. MOF/MSA-2(+)	ns	0.5003
MSA-2(+) vs. MOF(+)	*	0.0497
MSA-2(+) vs. MOF/MSA-2(+)	*	0.0191
MOF(+) vs. MOF/MSA-2(+)	ns	0.9966

b

Tukey's multiple comparisons test	Summary	Adjusted P Value
PBS vs. PBS(+)	ns	0.6568
PBS vs. MSA-2	ns	0.2035
PBS vs. MSA-2(+)	ns	0.0705
PBS vs. MOF(+)	*	0.0171
PBS vs. MOF/MSA-2(+)	**	0.0017
PBS(+) vs. MSA-2	ns	0.9433
PBS(+) vs. MSA-2(+)	ns	0.6793
PBS(+) vs. MOF(+)	ns	0.2916
PBS(+) vs. MOF/MSA-2(+)	*	0.041
MSA-2 vs. MSA-2(+)	ns	0.9905
MSA-2 vs. MOF(+)	ns	0.7856
MSA-2 vs. MOF/MSA-2(+)	ns	0.2132
MSA-2(+) vs. MOF(+)	ns	0.9792
MSA-2(+) vs. MOF/MSA-2(+)	ns	0.4925
MOF(+) vs. MOF/MSA-2(+)	ns	0.8781

c

Tukey's multiple comparisons test	Summary	Adjusted P Value
PBS vs. PBS(+)	ns	0.1794
PBS vs. MSA-2	ns	0.9842
PBS vs. MSA-2(+)	*	0.0331
PBS vs. MOF(+)	**	0.0037
PBS vs. MOF/MSA-2(+)	****	<0.0001
PBS(+) vs. MSA-2	ns	0.4738
PBS(+) vs. MSA-2(+)	ns	0.9427
PBS(+) vs. MOF(+)	ns	0.4081
PBS(+) vs. MOF/MSA-2(+)	**	0.0048
MSA-2 vs. MSA-2(+)	ns	0.1187
MSA-2 vs. MOF(+)	*	0.0148
MSA-2 vs. MOF/MSA-2(+)	***	0.0001
MSA-2(+) vs. MOF(+)	ns	0.8941
MSA-2(+) vs. MOF/MSA-2(+)	*	0.0309
MOF(+) vs. MOF/MSA-2(+)	ns	0.2195

d

Tukey's multiple comparisons test	Summary	Adjusted P Value
PBS vs. PBS(+)	ns	0.9068
PBS vs. MSA-2	ns	>0.9999
PBS vs. MSA-2(+)	ns	0.9925
PBS vs. MOF(+)	ns	0.4963
PBS vs. MOF/MSA-2(+)	*	0.0439
PBS(+) vs. MSA-2	ns	0.8777
PBS(+) vs. MSA-2(+)	ns	0.6239
PBS(+) vs. MOF(+)	ns	0.9686
PBS(+) vs. MOF/MSA-2(+)	ns	0.2732
MSA-2 vs. MSA-2(+)	ns	0.9963
MSA-2 vs. MOF(+)	ns	0.4516
MSA-2 vs. MOF/MSA-2(+)	*	0.0376
MSA-2(+) vs. MOF(+)	ns	0.226
MSA-2(+) vs. MOF/MSA-2(+)	*	0.014
MOF(+) vs. MOF/MSA-2(+)	ns	0.6954

Table S3. (a-c) p-value for Figure 5 d-f.

a

Tukey's multiple comparisons test	Summary	Adjusted P Value
PBS vs. PBS(+)	ns	0.7925
PBS vs. PD-L1(+)	ns	0.277
PBS vs. MOF/MSA-2(+)	**	0.0011
PBS vs. MOF/MSA-2(+)+αPD-L1	***	0.0005
PBS(+) vs. PD-L1(+)	ns	0.8685
PBS(+) vs. MOF/MSA-2(+)	**	0.0092
PBS(+) vs. MOF/MSA-2(+)+αPD-L1	**	0.0038
PD-L1(+) vs. MOF/MSA-2(+)	ns	0.0573
PD-L1(+) vs. MOF/MSA-2(+)+αPD-L1	*	0.0242
MOF/MSA-2(+) vs. MOF/MSA-2(+)+αPD-L1	ns	0.99

b

Tukey's multiple comparisons test	Summary	Adjusted P Value
PBS vs. PBS(+)	**	0.0037
PBS vs. PD-L1(+)	**	0.0036
PBS vs. MOF/MSA-2(+)	**	0.0065
PBS vs. MOF/MSA-2(+)+αPD-L1	**	0.0023
PBS(+) vs. PD-L1(+)	ns	>0.9999
PBS(+) vs. MOF/MSA-2(+)	ns	0.9983
PBS(+) vs. MOF/MSA-2(+)+αPD-L1	ns	0.999
PD-L1(+) vs. MOF/MSA-2(+)	ns	0.998
PD-L1(+) vs. MOF/MSA-2(+)+αPD-L1	ns	0.9992
MOF/MSA-2(+) vs. MOF/MSA-2(+)+αPD-L1	ns	0.9817

c

Tukey's multiple comparisons test	Summary	Adjusted P Value
PBS vs. PBS(+)	ns	0.9257
PBS vs. PD-L1(+)	ns	0.0901
PBS vs. MOF/MSA-2(+)	ns	0.8336
PBS vs. MOF/MSA-2(+)+αPD-L1	*	0.0221
PBS(+) vs. PD-L1(+)	ns	0.3291
PBS(+) vs. MOF/MSA-2(+)	ns	0.9992
PBS(+) vs. MOF/MSA-2(+)+αPD-L1	ns	0.0985
PD-L1(+) vs. MOF/MSA-2(+)	ns	0.4482
PD-L1(+) vs. MOF/MSA-2(+)+αPD-L1	ns	0.9401
MOF/MSA-2(+) vs. MOF/MSA-2(+)+αPD-L1	ns	0.1479

Table S4. (a-c) p-value for Figure 5 g-i.

a

Tukey's multiple comparisons test	Summary	Adjusted P Value
PBS vs. PBS(+)	ns	0.6191
PBS vs. PD-L1(+)	ns	0.977
PBS vs. MOF/MSA-2(+)	*	0.0427
PBS vs. MOF/MSA-2(+)+αPD-L1	ns	0.1624
PBS(+) vs. PD-L1(+)	ns	0.9082
PBS(+) vs. MOF/MSA-2(+)	**	0.0027
PBS(+) vs. MOF/MSA-2(+)+αPD-L1	*	0.0116
PD-L1(+) vs. MOF/MSA-2(+)	*	0.0143
PD-L1(+) vs. MOF/MSA-2(+)+αPD-L1	ns	0.0592
MOF/MSA-2(+) vs. MOF/MSA-2(+)+αPD-L1	ns	0.9411

b

Tukey's multiple comparisons test	Summary	Adjusted P Value
PBS vs. PBS(+)	ns	0.3626
PBS vs. PD-L1(+)	*	0.0457
PBS vs. MOF/MSA-2(+)	***	0.0003
PBS vs. MOF/MSA-2(+)+αPD-L1	****	<0.0001
PBS(+) vs. PD-L1(+)	ns	0.7268
PBS(+) vs. MOF/MSA-2(+)	**	0.0098
PBS(+) vs. MOF/MSA-2(+)+αPD-L1	**	0.0014
PD-L1(+) vs. MOF/MSA-2(+)	ns	0.1023
PD-L1(+) vs. MOF/MSA-2(+)+αPD-L1	*	0.0149
MOF/MSA-2(+) vs. MOF/MSA-2(+)+αPD-L1	ns	0.8383

c

Tukey's multiple comparisons test	Summary	Adjusted P Value
PBS vs. PBS(+)	ns	0.5566
PBS vs. PD-L1(+)	*	0.025
PBS vs. MOF/MSA-2(+)	***	0.0004
PBS vs. MOF/MSA-2(+)+αPD-L1	***	0.0005
PBS(+) vs. PD-L1(+)	ns	0.3502
PBS(+) vs. MOF/MSA-2(+)	**	0.0066
PBS(+) vs. MOF/MSA-2(+)+αPD-L1	**	0.0087
PD-L1(+) vs. MOF/MSA-2(+)	ns	0.2221
PD-L1(+) vs. MOF/MSA-2(+)+αPD-L1	ns	0.2767
MOF/MSA-2(+) vs. MOF/MSA-2(+)+αPD-L1	ns	0.9999

3. References

[1] D. Alezi, I. Spanopoulos, C. Tsangarakis, A. Shkurenko, K. Adil, Y. Belmabkhout, O. K. M, M. Eddaoudi, P. N. Trikalitis, *J Am Chem Soc* **2016**, *138*, 12767-12770.

[2] J. Liu, X. Jiang, Y. Li, K. Yang, R. R. Weichselbaum, W. Lin, *ACS Nano* **2024**, *18*, 5152-5166.

[3] J. S. Qin, S. Yuan, L. Zhang, B. Li, D. Y. Du, N. Huang, W. Guan, H. F. Drake, J. D. Pang, Y. Q. Lan, A. Alsalme, H. C. Zhou, *J Am Chem Soc* **2019**, *141*, 2054-2060.